and Ti$_2$Ni incoherently precipitate in the B2 matrix upon cooling from 700°C to 87°C. The B2 matrix transforms completely to B19 upon further cooling to 22°C, aided by the simultaneous Ti$_2$Cu/B19 epitaxies (Figs. 3 and 4, Table 1, and table S3). The B19/Ti$_2$Cu epitaxy provides an internal stress pattern, which stabilizes the B19 phase at low temperatures. During stress cycling, the equivalent epitaxy alternatingly stabilizes the B2 phase. At each temperature and stress, the transforming phases attain equilibrium by forming a compatible morphology directed by the internal epitaxy-generated stress distribution. Complete transformation is attained at each cycle because the epitaxial stresses are reversible. Hence, we propose that the epitaxially promoted completion of the B2↔B19 phase transformation creates the low-fatigue state of the Ti$_{54}$Ni$_{34}$Cu$_{12}$ films. The Ti$_2$Cu precipitates act like sentinels, assuring that the B2↔B19 transformation proceeds toward completion at each cycle. The transformation will return the film to a stress state and morphology that are compatible with the pristine state. The decrease of the anisotropic peak broadening of the epitaxy-effected XRD peaks indicates trainability.

This proposal must be revisited in light of the favorable values of the quantitative compatibility criteria calculated from the lattice parameters of both alloys Ti$_{51}$Ni$_{36}$Cu$_{13}$ and Ti$_{54}$Ni$_{34}$Cu$_{12}$ (Table 2). These values approach the ideal triplet ($\lambda = 1$, CCI = CCII = 0) and suggest good reversibility even in polycrystals (29), although they are inferior to those for Zn$_{45}$Au$_{30}$Cu$_{25}$ (19). The values for sample 2 are closer to the ideal than those for sample 1, which is in accord with the vastly better fatigue characteristics of sample 2. The question then arises whether this large difference of the fatigue life results from the observed epitaxy or that of the two triplets listed in Table 2. We observe that despite their reversibility, the phase transformations in SMAs are of first order (nucleation- and growth-controlled). We suggest that the epitaxy leads to reversible nucleation, whereas the low cofactors promote reversible near-equilibrium growth so that the combination of both mechanisms yields the observed ultralow fatigue. In the limit of CCI and CCII→0, no energy will be stored in the product phase in the form of twin boundaries. This creates a strongly reproducible, and therefore repeatably transformable, equilibrium state.

Given the fatigue-controlling importance of the dual epitaxy of Ti$_2$Cu in TiNiCu-based (SMA) films, it is natural to search for other alloying elements that have the potential to play a similar role. Following this lead, we can assume that structurally related Ti$_2$Ag precipitates will act very similar to Ti$_2$Cu. Because TiNiAg SMAs display transformation characteristics comparable with that of TiNiCu (30), they could be promising candidates for biocompatible ultralow fatigue SMA films. Elastocaloric cooling requires bulk materials, which is a difficult but, in principle, solvable challenge. More generally, we expect similar behavior in phase-transforming materials that contain dual-epitaxial precipitates.

REFERENCES AND NOTES

1. K. Otsuka, X. Ren, *Prog. Mater. Sci.* **50**, 511–678 (2005).
2. J. Mohd Jani, M. Leary, A. Subic, M. A. Gibson, *Mater. Des.* **56**, 1078–1113 (2014).
3. T. Duerig, A. Pelton, D. Stöckel, *Mater. Sci. Eng. A* **273–275**, 149–160 (1999).
4. D. W. Raboud, M. G. Faulkner, A. W. Lipsett, *Smart Mater. Struct.* **9**, 684–692 (2000).
5. E. Bonnot, R. Romero, L. Mañosa, E. Vives, A. Planes, *Phys. Rev. Lett.* **100**, 125901 (2008).
6. K. Otsuka, C. M. Wayman, Eds., *Shape Memory Materials* (Cambridge Univ. Press, Cambridge, 1999).
7. J. Cui et al., *Nat. Mater.* **5**, 286–290 (2006).
8. K. Bhattacharya, S. Conti, G. Zanzotto, J. Zimmer, *Nature* **428**, 55–59 (2004).
9. X. Moya, S. Kar-Narayan, N. D. Mathur, *Nat. Mater.* **13**, 439–450 (2014).
10. W. J. Buehler, J. V. Gilfrich, R. C. Wiley, *J. Appl. Phys.* **34**, 1475–1477 (1963).
11. S. A. Shabalovskaya, *Biomed. Mater. Eng.* **12**, 69–109 (2002).
12. N. B. Morgan, *Mater. Sci. Eng. A* **378**, 16–23 (2004).
13. A. R. Pelton, *J. Mater. Eng. Perform.* **20**, 613–617 (2011).
14. G. Eggeler, E. Hornbogen, A. Yawny, A. Heckmann, M. Wagner, *Mater. Sci. Eng. A* **378**, 24–33 (2004).
15. S. Miyazaki, K. Mizukoshi, T. Ueki, T. Sakuma, Y. Liu, *Mater. Sci. Eng. A* **273–275**, 658–663 (1999).
16. E. Hornbogen, *J. Mater. Sci.* **39**, 385–399 (2004).
17. K. Gall, H. J. Maier, *Acta Mater.* **50**, 4643–4657 (2002).
18. R. D. James, Z. Zhang, in *Magnetism and Structure in Functional Materials*, A. Planes, L. Manosa, A. Saxena, Eds. (Springer, New York, 2005), vol. 79.
19. Y. Song, X. Chen, V. Dabade, T. W. Shield, R. D. James, *Nature* **502**, 85–88 (2013).
20. S. Miyazaki, Y. Q. Fu, W. M. Huang, Eds., *Thin Film Shape Memory Alloys* (Cambridge Univ. Press, Cambridge, 2009).
21. K. Bhattacharya, R. D. James, *Science* **307**, 53–54 (2005).
22. C. Bechtold, C. Chluba, R. Lima de Miranda, E. Quandt, *Appl. Phys. Lett.* **101**, 091903 (2012).
23. R. Lima de Miranda, C. Zamponi, E. Quandt, *Adv. Eng. Mater.* **15**, 66–69 (2013).
24. G. Siekmeyer, A. Schüßler, R. de Miranda, E. Quandt, *J. Mater. Eng. Perform.* **23**, 2437–2445 (2014).
25. Materials and methods are available as supplementary materials on *Science* Online.
26. K. Bhattacharya, *Microstructure of Martensite: Why It Forms and How It Gives Rise to the Shape-Memory Effect* (Oxford Univ. Press, Oxford, 2003).
27. A. C. Larson, R. B. Von Dreele, "General Structure Analysis System (GSAS)," Los Alamos National Laboratory Report LAUR 86-748 (2004).
28. P. Stephens, *J. Appl. Cryst.* **32**, 281–289 (1999).
29. K. Bhattacharya, R. V. Kohn, *Acta Mater.* **44**, 529–542 (1996).
30. C. Zamponi, M. Wuttig, E. Quandt, *Scripta Mater.* **56**, 1075–1077 (2007).
31. H. Scott, *J. Appl. Cryst.* **16**, 159–163 (1983).

MEMORY

Engram cells retain memory under retrograde amnesia

Tomás J. Ryan,[1,2]* Dheeraj S. Roy,[1]* Michele Pignatelli,[1] Autumn Arons,[1,2] Susumu Tonegawa[1,2]†

Memory consolidation is the process by which a newly formed and unstable memory transforms into a stable long-term memory. It is unknown whether the process of memory consolidation occurs exclusively through the stabilization of memory engrams. By using learning-dependent cell labeling, we identified an increase of synaptic strength and dendritic spine density specifically in consolidated memory engram cells. Although these properties are lacking in engram cells under protein synthesis inhibitor–induced amnesia, direct optogenetic activation of these cells results in memory retrieval, and this correlates with retained engram cell–specific connectivity. We propose that a specific pattern of connectivity of engram cells may be crucial for memory information storage and that strengthened synapses in these cells critically contribute to the memory retrieval process.

Memory consolidation is the phenomenon by which a newly formed memory transitions from a fragile state to a stable, long-term state (1–3). The defining feature of consolidation is a finite time window that begins immediately after learning, during which a memory is susceptible to disruptions, such as protein synthesis inhibition (4–6), resulting in retrograde amnesia. The stabilization of synaptic potentiation is the dominant cellular model of memory consolidation (7–10) because protein synthesis inhibitors disrupt late-phase

long-term potentiation of in vitro slice preparations (11–13). Although much is known about the cellular mechanisms of memory consolidation, it remains unknown whether these processes occur in memory engram cells. It may be possible to characterize cellular consolidation and empirically separate mnemonic properties in retrograde amnesia by directly probing and manipulating memory engram cells in the brain. The term memory engram originally referred to

[1]RIKEN-MIT Center for Neural Circuit Genetics at the Picower Institute for Learning and Memory, Department of Biology and Department of Brain and Cognitive Sciences, Massachusetts Institute of Technology, Cambridge, MA 02139, USA. [2]Howard Hughes Medical Institute, Massachusetts Institute of Technology, Cambridge, MA 02139, USA.
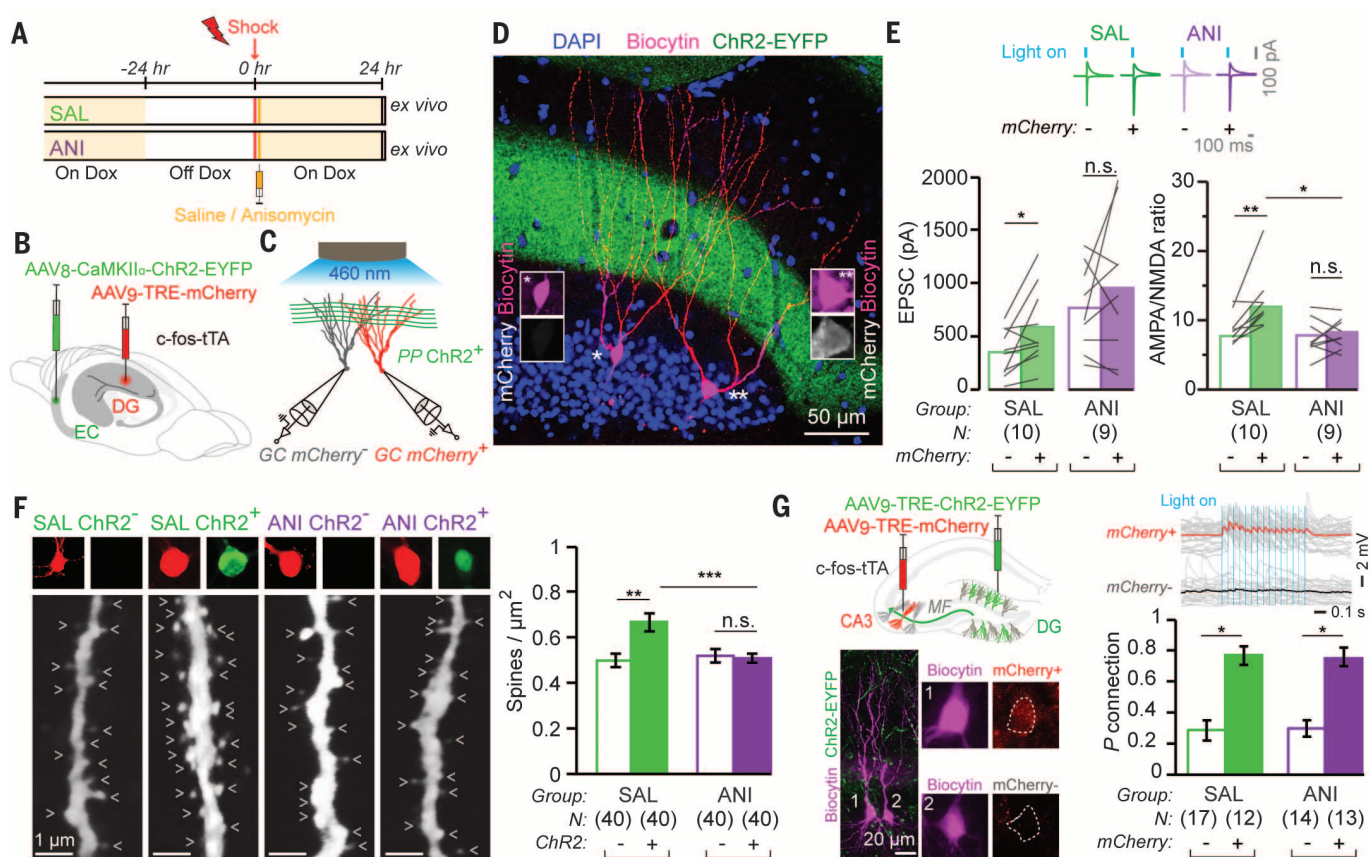*These authors contributed equally to this work. †Corresponding author. E-mail: tonegawa@mit.edu

the hypothetical learned information stored in the brain, which must be reactivated for recall (14, 15). Recently, several groups demonstrated that specific hippocampal cells that are activated during memory encoding are both sufficient (16–18) and necessary (19, 20) for driving future recall of a contextual fear memory and thus represent a component of a distributed memory engram (21). Here, we applied this engram technology to the issue of cellular consolidation and retrograde amnesia.

We used the previously established method for tagging the hippocampal dentate gyrus (DG) component of a contextual memory engram with mCherry (supplementary materials, materials and methods, and fig. S1) (16, 22). To disrupt consolidation, we systemically injected the protein synthesis inhibitor anisomycin (ANI) or saline (SAL)

as a control immediately after contextual fear conditioning (CFC) (Fig. 1A). The presynaptic neurons of the entorhinal cortex (EC) were constitutively labeled with ChR2 expressed from an AAV$_8$-CaMKIIα-ChR2-EYFP virus (Fig. 1B). Voltage clamp recordings of paired engram (mCherry$^+$) and nonengram (mCherry$^-$) DG cells were conducted simultaneously with optogenetic stimulation of ChR2$^+$ perforant path (PP) axons (Fig. 1, C and D). mCherry$^+$ cells of the SAL group showed significantly greater synaptic strength than did paired mCherry$^-$ cells, whereas in the ANI group, mCherry$^+$ and mCherry$^-$ cells were of comparable synaptic strength (Fig. 1E). Calculation of AMPA/N-methyl-D-aspartate (NMDA) receptor current ratios (23) showed that at 24 hours after training, mCherry$^+$ engram cells displayed potentiated synapses relative to paired mCherry$^-$ non-engram

Fig. 1. Synaptic plasticity and connectivity of engram cells. (**A**) Mice taken off doxycycline (DOX) 24 hours before CFC and dispatched 24 hours after training. SAL or ANI was administered immediately after training. (**B**) AAV$_8$-CaMKIIα-ChR2-EYFP and AAV$_9$-TRE-mCherry viruses injected into the entorhinal cortex and dentate gyrus, respectively, of c-Fos-tTA mice. (**C**) Paired recordings of engram (red) and nonengram (gray) DG cells during optogenetic stimulation of ChR2$^+$ PP axons. (**D**) Representative image of a pair of recorded biocytin-labeled engram (mCherry$^+$) and nonengram (mCherry$^-$) DG cells. ChR2$^+$ PP axons are in green. (**E**) (Top) Example traces of AMPA and NMDA receptor–dependent postsynaptic currents in mCherry$^+$ and mCherry$^-$ cells, evoked by means of light activation of ChR2$^+$ PP axons. (Bottom) EPSC amplitudes and AMPA/NMDA current ratios of mCherry$^+$ and mCherry$^-$ cells of the two groups are displayed as means (columns) and individual paired data points (gray lines). Paired *t* test; *P < 0.05, **P < 0.001. SAL group

compared with the ANI group, unpaired *t* test; *P < 0.05. (**F**) (Left) Representative confocal images of biocytin-filled dendritic fragments derived from SAL and ANI groups for ChR2$^+$ and ChR2$^-$ cells (arrow heads indicate dendritic spines). (Right) Average dendritic spine density showing an increase occurring exclusively in ChR2$^+$ fragments. Data are represented as mean ± SEM. Unpaired *t* tests **P < 0.01, ***P < 0.001. (**G**) Engram connectivity. (Top left) AAV$_9$-TRE-ChR2-EYFP and AAV$_9$-TRE-mCherry viruses, injected into the DG and CA3, respectively, of c-Fos-tTA mice. (Bottom left) Example of mCherry$^+$ (1) and mCherry$^-$ (2) biocytin-filled CA3 pyramidal cells. ChR2$^+$ mossy fibers (MF) are in green. (Top right) mCherry$^+$ cell but not mCherry$^-$ cell displayed excitatory postsynaptic potentials in response to optogenetic stimulation of MF. (Bottom right) Probability of connection of DG ChR2$^+$ engram axons and CA3 mCherry$^+$ and mCherry$^-$ cells. Error bars are approximated by using binomial distribution. Fisher's exact test; *P < 0.05.

cells in the SAL group (Fig. 1E). However, no such difference between mCherry⁺ and mCherry⁻ was observed in the ANI group. In addition, mCherry⁺ engram cells of the SAL group showed significantly greater AMPA/NMDA current ratios than those of mCherry⁺ engram cells of the ANI group. Analysis of spontaneous excitatory postsynaptic currents (EPSCs) of engram and non-engram cells of both SAL and ANI groups showed the same pattern (fig. S2).

We also quantified dendritic spine density for DG engram cells labeled with an AAV₉-TRE-ChR2-EYFP virus. Spine density of ChR2⁺ cells was significantly higher than corresponding ChR2⁻ cells in the SAL group (Fig. 1F and fig. S3), but spine densities of ChR2⁺ and ChR2⁻ cells of the ANI group were similar (supplementary materials, materials and methods). Spine density of ChR2⁺ cells of the SAL group was significantly higher than that of ANI ChR2⁺ cells (Fig. 1F), but ChR2⁻ cell spine density was comparable. This result was confirmed with analysis of the membrane capacitance (fig. S4G). ChR2 expression did not affect intrinsic properties of DG cells in vitro (fig. S5, A to E). Direct bath application of ANI did not affect intrinsic cellular properties in vitro (fig. S5F), although it mildly reduced synaptic currents acutely (fig. S5, G to I). When ANI was injected into c-Fos-tTA animals 24 hours after CFC and engram labeling, engram cell–specific increases in dendritc spine density and synaptic strength were undisturbed (fig. S6). We also examined engram cells labeled by means of a context-only experience (17) and found equivalent engram-cell increases in spine density and synaptic strength (fig. S7) as those labeled by means of CFC.

DG cells receive information from EC and relay it to CA3 via the mossy fiber pathway. We labeled DG engram cells using an AAV₉-TRE-ChR2-EYFP virus and simultaneously labeled CA3 engram cells using an AAV₉-TRE-mCherry virus (Fig. 1G). Connection probability was assessed 24 hours after CFC by stimulating DG ChR2⁺ cell terminals optogenetically and recording excitatory postsynaptic potentials in CA3 mCherry⁺ and mCherry⁻ cells in ex vivo preparations. CA3 mCherry⁺ engram cells showed a significantly higher probability of connection than did mCherry⁻ cells with DG ChR2⁺ engram cells, demonstrating preferential engram cell–to–engram cell connectivity. This form of engram pathway–specific connectivity was unaffected by posttraining administration of ANI (Fig. 1G).

We next tested the behavioral effect of optogenetically stimulating engram cells in amnesic mice (Fig. 2A). During CFC training in context B, both SAL and ANI groups responded to the unconditioned stimuli at equivalent levels (fig. S8). One day after training, the SAL group displayed robust freezing behavior to the conditioned stimulus of context B, whereas the ANI group showed substantially less freezing behavior (Fig. 2C). Two days after training, mice were placed into the distinct context A for a 12-min test session consisting of four 3-min epochs of blue light on or off. During this test session, neither group showed freezing behavior during light-off epochs, but both froze significantly during light-on epochs (Fig. 2D). Remarkably, no difference in the levels of light-induced freezing behavior was observed between groups. Three days after training, the mice were again tested in context B in order to assay the conditioned response, and retrograde amnesia for the conditioning context was still clearly evident (Fig. 2E). Subjects treated with SAL or ANI after the labeling of a neutral contextual engram (no shock) did not show freezing behavior in response to light stimulation of engram cells (Fig. 2D). We replicated the DG retrograde amnesia experiment using an alternative widely used protein synthesis inhibitor, cycloheximide (CHM)
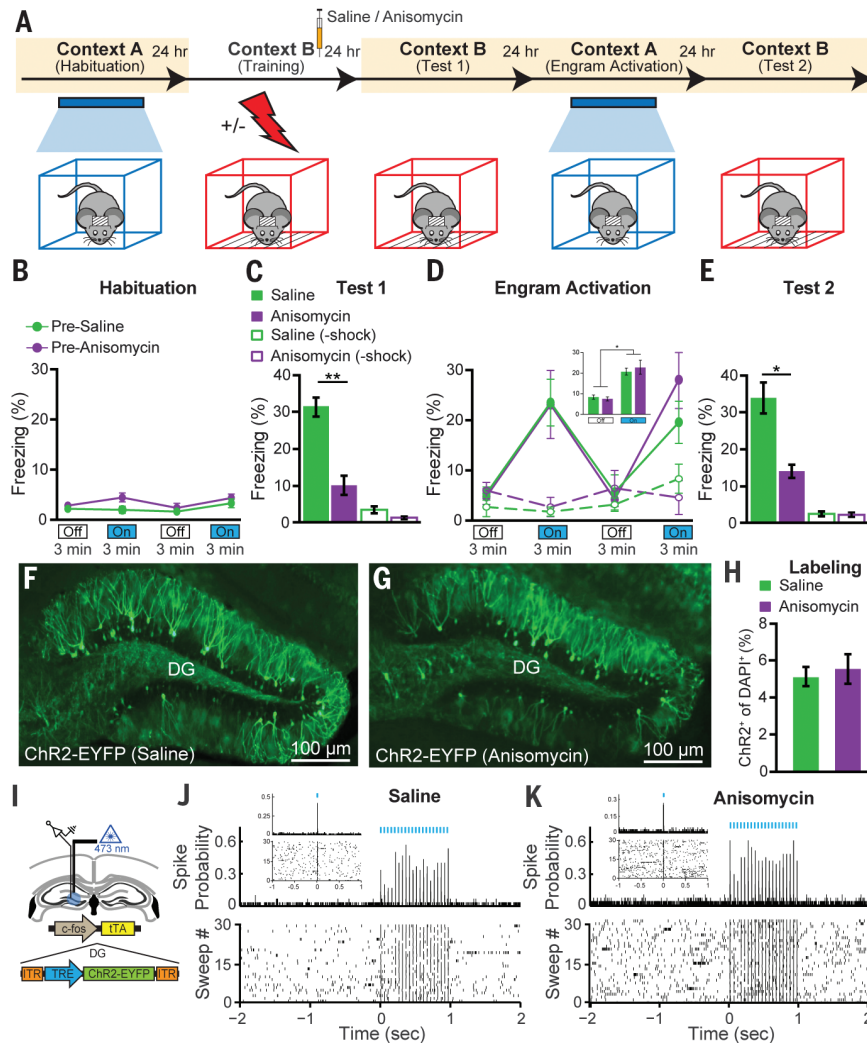

Fig. 2. Optogenetic stimulation of DG engram cells restores fear memory in retrograde amnesia.
(**A**) Behavioral schedule. Beige shading signifies that subjects are on DOX, precluding ChR2 expression. Mice are taken off DOX 24 to 30 hours before CFC in context B. SAL or ANI was injected into the mice after training. (**B**) Habituation to context A with light-off and light-on epochs. Blue light stimulation of the DG did not cause freezing behavior in naïve, unlabeled mice of the pre-SAL ($n = 10$ mice) or pre-ANI ($n = 8$ mice) groups. (**C**) Memory recall in context B 1 day after training (test 1). ANI group displayed significantly less freezing than SAL group ($P < 0.005$). No-shock groups with SAL ($n = 4$ mice) or ANI ($n = 4$ mice) did not display freezing upon reexposure to context B. (**D**) Memory recall in context A 2 days after training (engram activation) with light-off and light-on epochs. Freezing for the two light-off and light-on epochs are further averaged in the inset. Significant freezing due to light stimulation was observed in both the SAL ($P < 0.01$) and ANI groups ($P < 0.05$). Freezing levels did not differ between groups. SAL and ANI-treated no-shock control groups did not freeze in response to light stimulation of context B engram cells. (**E**) Memory recall in context B 3 days after training (test 2). ANI group displayed significantly less freezing than SAL group ($P < 0.05$). (**F** and **G**) Images showing DG sections from c-Fos-tTA mice 24 hours after SAL or ANI treatment. (**H**) ChR2-EYFP cell counts from DG sections of SAL ($n = 3$ mice) and ANI ($n = 4$ mice) groups. (**I**) In vivo anesthetized recordings (supplementary materials, materials and methods). (**J** and **K**) Light pulses induced spikes in DG neurons recorded from head-fixed anesthetized c-Fos-tTA mice 24 hours after treatment with either SAL or ANI. Data are presented as mean ± SEM.

(fig. S9). We examined whether ANI administration immediately after CFC altered the activity-dependent synthesis of ChR2-EYFP in DG cells and found that this was not the case (Fig. 2, F to H). Nevertheless, the dosage of ANI used in this study did inhibit protein synthesis in the DG, as shown with Arc[+] cell counting (fig. S10). Thus, the dosage of ANI used was sufficient to induce amnesia but was insufficient to impair c-Fos–tTA–driven synthesis of virally delivered ChR2-EYFP in DG cells. Extracellular recordings from SAL- and ANI-treated mice confirmed the cell counting results (Fig. 2, I to K). In line with fig. S6 and previous reports (24), ANI injection 24 hours after CFC did not cause retrograde amnesia (fig. S11). To provide a negative control for light-induced memory retrieval in amnesia, we disrupted memory encoding by activating hM4Di DREADDs receptors (25) downstream of the DG, in hippocampal CA1, during CFC, and found that subsequent DG engram activation did not elicit memory retrieval (fig. S12).

The recovery from amnesia through the direct light activation of ANI-treated DG engram cells was unexpected because these cells showed neither synaptic potentiation nor increased dendritic spine density. We conducted additional behavioral experiments in order to confirm and characterize the phenomenon. First, we investigated whether recovery from amnesia can be demonstrated by means of light-induced optogenetic place avoidance test (OptoPA); this would be a measure of an active fear memory recall (supplementary materials, materials and methods) (18), rather than a passive fear response monitored with freezing. SAL and ANI groups displayed equivalent levels of avoidance of target zone in response to light activation of the DG engram (Fig. 3A). Second, in our previous study we showed that an application of the standard protocol (20 Hz) for activation of the CA1 engram was not effective for memory recall (17). However, we found that a 4-Hz protocol applied to the CA1 engram of the SAL and ANI groups

elicited similar recovery from amnesia (Fig. 3B). Third, we used tone fear conditioning (TFC) and manipulated the fear engram in lateral amygdala (LA) (26) and found light-induced recovery of memory from amnesia. Fourth, we asked whether amnesia caused by disruption of reconsolidation of a contextual fear memory (27, 28) can also be recovered through the light-activation of DG engram cells, which was found to be the case (Fig. 4A). We applied the memory inception method (supplementary materials, materials and methods) (17, 29) to DG engram cells and found that both SAL and ANI groups showed freezing behavior that was specific to the original context A, demonstrating that light-activated context A engrams formed in the presence of ANI can function as a conditioned stimulus (CS) in a context-specific manner (Fig. 4B). Last, we tested the longevity of CFC amnesic engrams for memory recovery by means of light activation and found that memory recall could be observed 8 days after training (fig. S13).
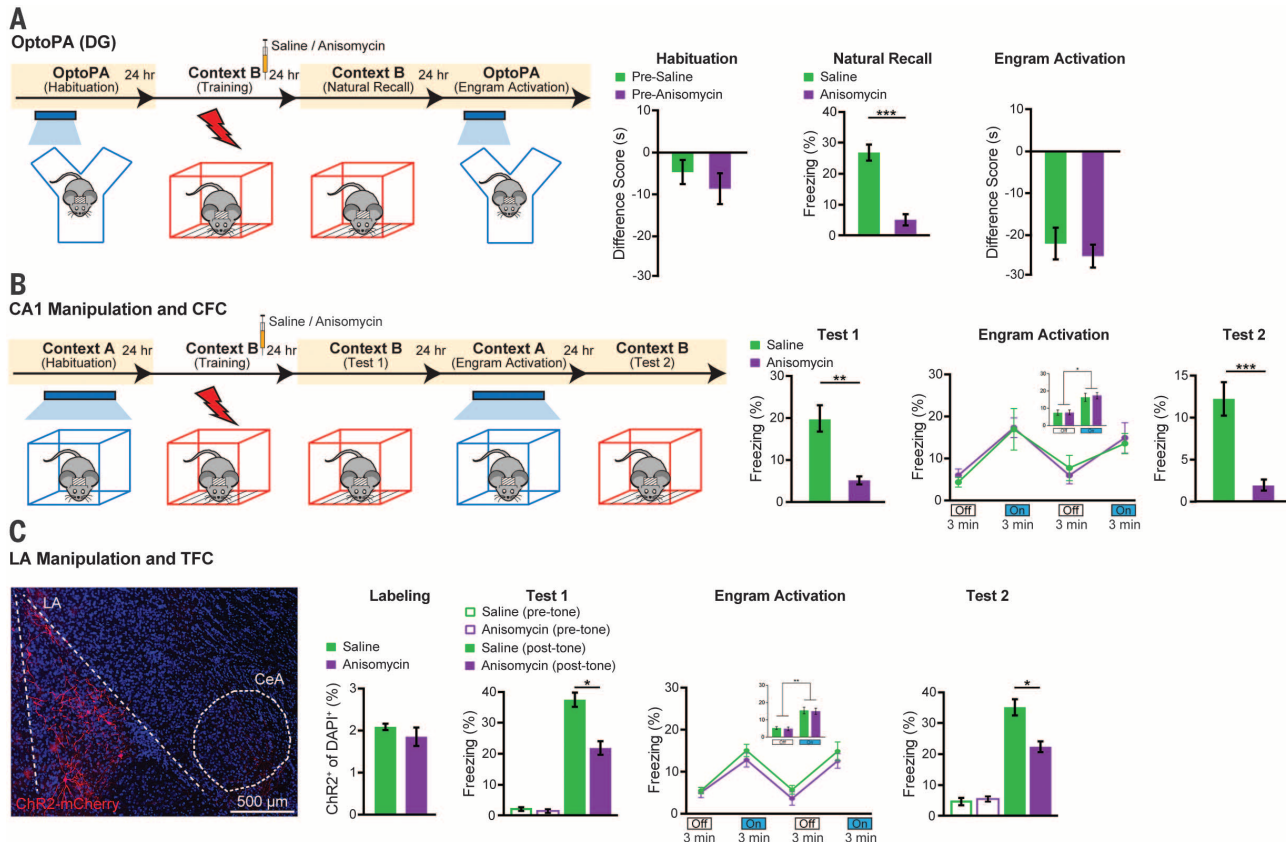
Fig. 3. Recovery of memory from amnesia under a variety of conditions. (**A**) DG engram activation and optogenetic place avoidance (OptoPA). During habituation, neither group displayed significant avoidance of target zone. For natural recall, the ANI group (n = 10 mice) displayed significantly less freezing than SAL group (n = 12 mice) in context B (P < 0.005). SAL and ANI groups displayed similar levels of OptoPA. (**B**) CA1 engram activation and CFC. 1 day after CFC (test 1), ANI group (n = 9 mice) displayed significantly less freezing than that of SAL group (n = 10 mice) in context B (P < 0.01). Two days after training (engram activation), light-activation of CA1 engrams elicited freezing in both SAL (P < 0.01) and ANI groups (P < 0.001). Three days after training (test 2), ANI group froze less than did SAL group in context B (P < 0.01). (**C**) LA engram activation and TFC. The behavioral schedule was identical to that in Fig. 3B, except that context tests were replaced with tone tests in context C (supplementary materials, materials and methods). (Left) Example image of ChR2-mCherry labeling of LA neurons. Of DAPI cells, 2% were labeled with ChR2. (Right) One day after training (test 1), ANI group (n = 9 mice) displayed significantly less freezing to tone than did SAL group (n = 9 mice) (P < 0.05). Two days after training (engram activation), significant light-induced freezing was observed for both SAL (P < 0.005) and ANI groups (P < 0.005). Three days after training (test 2), ANI group froze less to tone than did SAL group (P < 0.05).

Interactions between the hippocampus and amygdala are crucial for contextual fear memory encoding and retrieval (18). c-Fos expression increases in the hippocampus and amygdala upon exposure of an animal to conditioned stimuli (30, 31). These previous observations open up the possibility of obtaining cellular-level evidence to support the behavioral-level finding that the recovery from amnesia can be accomplished with direct light activation of ANI-treated DG engram cells. Thus, we compared the effects of natural recall and light-induced recall on amygdala c-Fos[+] cell counts in amnesic mice (Fig. 5, A to C). c-Fos[+] cell counts (Fig. 5B) were significantly lower in basolateral amygdala (BLA) and central amygdala (CeA) of ANI-treated mice as compared with SAL mice when natural recall cues were delivered, showing that amygdala activity correlates with fear memory expression (Fig. 5C). In contrast, light-induced activation of the contextual engram cells resulted in equivalent amygdala c-Fos[+] counts in SAL and ANI groups (Fig. 5C), which supports the optogenetic behavioral data.

Next, we modified this protocol in order to include labeling of CA3 and BLA engram cells with mCherry and examined the effects of light-induced activation of DG engram cells on the overlap of mCherry^{+} engram cells and c-Fos[+] recall-activated cells in CA3 and BLA (Fig. 5D). The purpose of this experiment was to investigate whether there is preferential connectivity between the upstream engram cells in DG and the downstream engram cells in CA3 or BLA. Natural recall cues resulted in above-chance c-Fos[+]/mCherry[+] overlap in both CA3 and BLA, which supports the physiological connectivity data (Fig. 5, E to K). c-Fos[+]/mCherry[+] overlap was significantly reduced in the ANI group as compared with the SAL group but was still higher than chance levels, presumably reflecting incomplete amnesic effects of ANI (Fig. 5K). Light-activation of DG engram cells resulted in equivalent c-Fos[+]/mCherry[+] overlap as natural cue-induced recall, and this was unaffected by post-CFC ANI treatment. These data suggest that there is preferential and protein synthesis–independent functional connectivity between DG and CA3 engram cells, which supports the physiological data (Fig. 1G), and that this connectivity also applies between DG and BLA engram cells.

We previously showed that DG cells activated during CFC training and labeled with ChR2 via the promoter of an immediate early gene (IEG) can evoke a freezing response when they are reactivated optogenetically 1 to 2 days later (16), and this has since been achieved in the cortex (21). We have also shown that these DG cells, if light-activated while receiving an unconditioned stimulus (US), can serve as a surrogate context-specific CS to create a false CS-US association (17, 18), and that activation of DG or amygdala engram cells can induce place preference (18). Furthermore, recent studies showed that optogenetic inhibition of these cells in DG, CA3, or CA1 impairs expression of a CFC memory (19, 20). Together, these findings show that engram cells activated through CFC training are both sufficient and necessary to evoke memory recall, satisfying two crucial attributes in defining a component of a contextual fear memory engram (15). What has been left to be demonstrated, however, is that these DG cells undergo enduring physical changes as an experience is encoded and its memory is consolidated. Although synaptic potentiation has long been suspected as a fundamental mechanism for memory and as a crucial component of the enduring physical changes induced by experience, this has not been directly demonstrated,
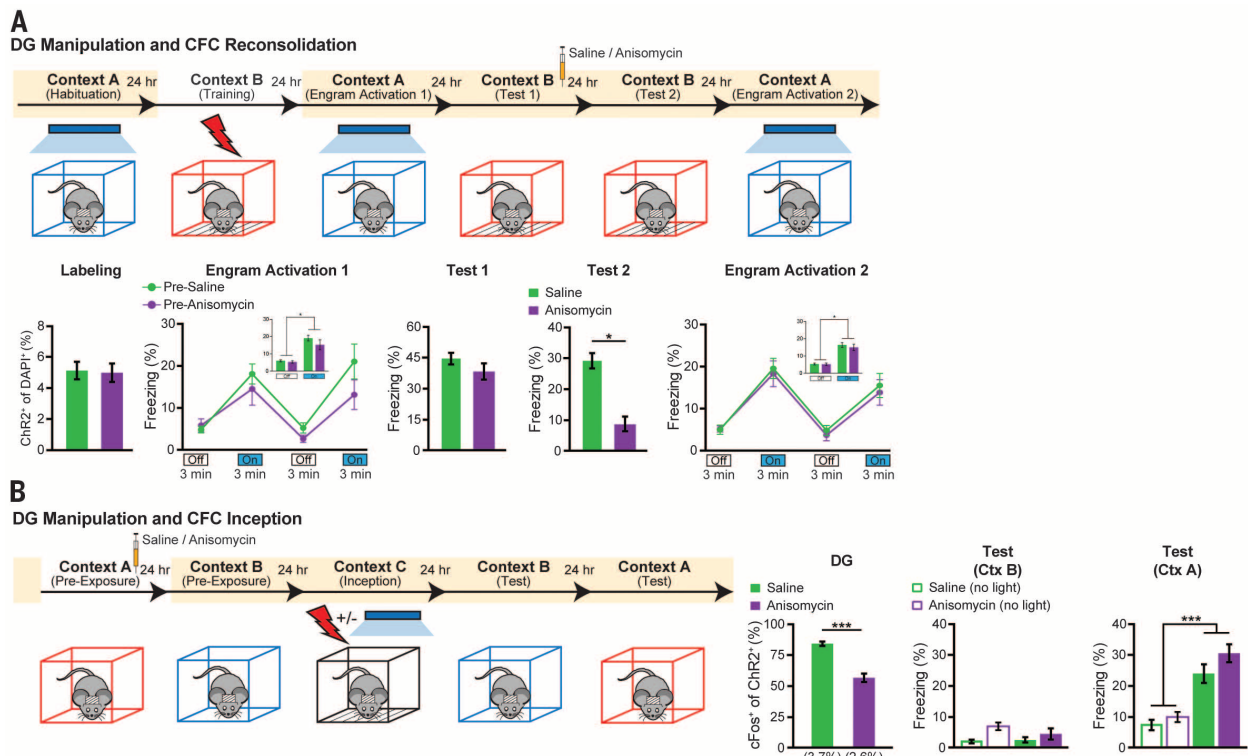
Fig. 4. Reconsolidation and memory updating. (**A**) DG engram activation and CFC reconsolidation. ANI (n = 11 mice) and SAL (n = 11 mice) groups showed similar levels of ChR2 labeling. Both groups showed light-induced freezing behavior 1 day after training (engram activation 1), pre-SAL (P < 0.001), pre-ANI (P < 0.02). Two days after training (test 1), the fear memory was reactivated by exposure to context B, and SAL or ANI was injected. Three days after training (test 2), the ANI group froze significantly less than did the SAL group to context B (P < 0.01). Four days after training (engram activation 2), significant light-induced freezing was observed for the SAL (P < 0.001) and ANI (P < 0.003) groups. (**B**) DG inception (supplementary materials, materials and methods) after contextual memory amnesia. Context-only engram was labeled for target context A, followed by injection of SAL (n = 11 mice) or ANI (n = 11 mice). Amnesia was demonstrated in the ANI group through decreased ChR2^{+}/c-Fos[+] colabeling after context A reexposure 1 day after labeling. After fear inception, neither SAL nor ANI groups displayed freezing behavior in context B, whereas both groups displayed significant freezing in context A, with no significant difference between groups. No-light inception SAL (n = 7 mice) and ANI (n = 6 mice) controls displayed no freezing to context A or B. Statistical comparisons are performed by using unpaired t tests; ***P < 0.001. Data are presented as mean ± SEM.

until the current study, as a property of the engram cells. Our data have directly linked the optogenetically and behaviorally defined memory engram cells to synaptic plasticity.

On the basis of a large volume of previous studies, (1–3, 7, 8, 32–34), a concept has emerged in which retrograde amnesia arises from consolidation failure as a result of disrupting the process that converts a fragile memory engram, formed during the encoding phase, into a stable engram with persistently augmented synaptic strength and spine density. Indeed, our current study has demonstrated that amnesic engram cells in the DG 1 day after CFC training display low levels of synaptic strength and spine density that are indistinguishable from nonengram cells of the same DG. This correlated with a lack of memory recall elicited by contextual cues.

Fig. 5. Amygdala activation and functional connectivity in amnesia through light activation of DG engram. (**A**) Schedule for cell-counting experiments. Mice were either given a natural recall session in context B or a light-induced recall session in context A. Mice were perfused 1 hour after recall. (**B**) Representative image showing c-Fos expression in the BLA and CeA. (**C**) c-Fos⁺ cell counts in the BLA and CeA of mice after natural or light-induced recall (n = 3 or 4 mice per group). (**D**) Schedule for cell-counting experiments. c-Fos-tTA mice with AAV₉-TRE-ChR2-EYFP injected into the DG and AAV₉-TRE-mCherry injected into both CA3 and BLA were fear-conditioned off DOX and 1 day later were given a natural recall session in context B or a light-induced recall session in context A. Mice were perfused 1 hour after recall. (**E** to **G**) Representative images showing mCherry engram cell labeling, c-Fos expression, and mCherry⁺/c-Fos⁺ overlap in CA3. (**H** to **J**) Representative images showing mCherry engram cell labeling, c-Fos expression, and mCherry/c-Fos overlap in BLA. (**K**) c-Fos⁺/mCherry⁺ overlap cell counts in CA3 and BLA of mice after natural or light-induced recall (n = 3 or 4 mice per group). Chance levels were estimated at 0.76 (CA3) and 0.42 (BLA). Data are presented as mean ± SEM. Statistical comparison are performed by using unpaired t tests; *$P < 0.05$, **$P < 0.01$.
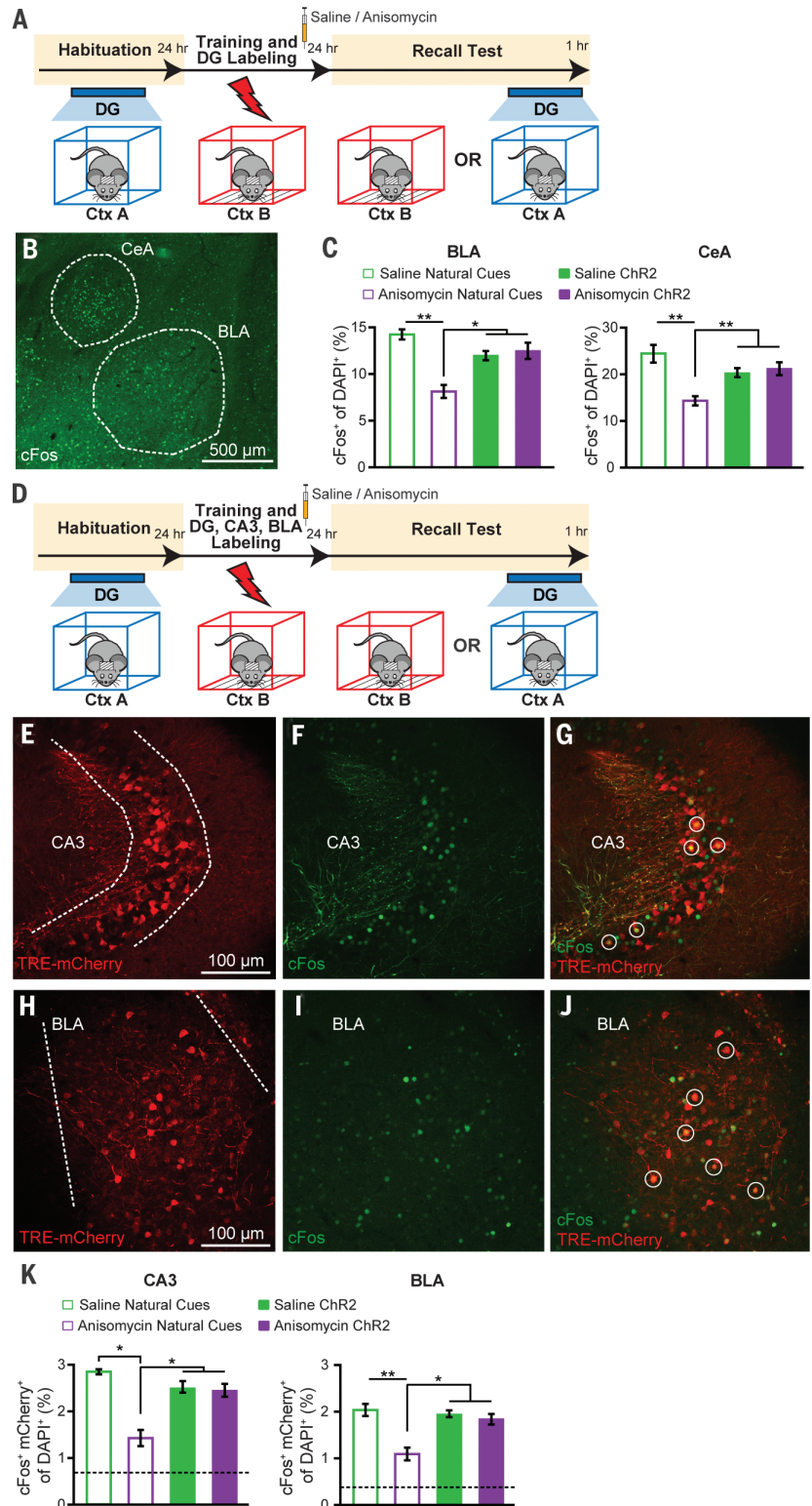
However, direct activation of DG engram cells of the ANI group elicited as much freezing behavior as did the activation of these cells of the SAL group. This unexpected finding is supported by a set of additional cellular and behavioral experiments. Whereas amygdala engram cell reactivation upon exposure to the conditioned context is significantly lower in the ANI group as compared with the SAL group, optogenetic activation of DG engram cells results in normal reactivation of downstream CA3 and BLA engram cells (Fig. 5). At the behavioral level, the amnesia rescue was observed under a variety of different conditions in which one or more parameters were altered (Figs. 2 and 3 and figs. S9 and S13). Thus, our overall findings indicate that memory engrams survive a posttraining administration of protein synthesis inhibitors during the consolidation window and that the memory remains retrievable by means of ChR2-mediated direct engram activation even after retrograde amnesia is induced. The drive initiated with light-activation of one component of a distributed memory engram (such as that in the DG) is sufficient to reactivate engrams in downstream regions (such as that in CA3 and BLA) that would also be affected by the systemic injection of a protein synthesis inhibitor (ANI).

These findings suggest that although a rapid increase of synaptic strength is likely to be crucial during the encoding phase, the augmented synaptic strength is not a crucial component of the stored memory (35–37). This perspective is consistent with a recent study showing that an artificial memory could be reversibly disrupted by depression of synaptic strength (38). On the other hand, persistent and specific connectivity of engram cells that we find between DG engram cells and downstream CA3 or BLA engram cells in both SAL and ANI groups may represent a fundamental mechanism of memory information storage (39). Our findings also suggest that the primary role of augmented synaptic strength during and after the consolidation phase may be to provide natural recall cues with efficient access to the soma of engram cells for their reactivation and, hence, recall.

The integrative memory engram-based approach used here for parsing memory and amnesia into encoding, consolidation, and retrieval aspects may be of wider use to other experimental and clinical cases of amnesia, such as Alzheimer's disease (40).

REFERENCES AND NOTES

1. G. E. Müller, A. Pilzecker, *Z. Psychol.* **1**, 1–288 (1900).
2. C. P. Duncan, *J. Comp. Physiol. Psychol.* **42**, 32–44 (1949).
3. J. L. McGaugh, *Science* **287**, 248–251 (2000).
4. J. B. Flexner, L. B. Flexner, E. Stellar, *Science* **141**, 57–59 (1963).
5. L. B. Flexner, J. B. Flexner, R. B. Roberts, *Science* **155**, 1377–1383 (1967).
6. H. P. Davis, L. R. Squire, *Psychol. Bull.* **96**, 518–559 (1984).
7. E. R. Kandel, *Science* **294**, 1030–1038 (2001).
8. R. J. Kelleher 3rd, A. Govindarajan, S. Tonegawa, *Neuron* **44**, 59–73 (2004).
9. T. Takeuchi, A. J. Duszkiewicz, R. G. Morris, *Philos. Trans. R. Soc. Lond. B Biol. Sci.* **369**, 20130288 (2014).
10. A. Govindarajan, I. Israely, S. Y. Huang, S. Tonegawa, *Neuron* **69**, 132–146 (2011).
11. M. Krug, B. Lössner, T. Ott, *Brain Res. Bull.* **13**, 39–42 (1984).
12. U. Frey, M. Krug, K. G. Reymann, H. Matthies, *Brain Res.* **452**, 57–65 (1988).
13. Y. Y. Huang, P. V. Nguyen, T. Abel, E. R. Kandel, *Learn. Mem.* **3**, 74–85 (1996).
14. R. Semon, *Die Mneme als erhaltendes Prinzip im Wechsel des organischen Geschehens* (Wilhelm Engelmann, Leipzig, 1904).
15. S. A. Josselyn, *J. Psychiatry Neurosci.* **35**, 221–228 (2010).
16. X. Liu et al., *Nature* **484**, 381–385 (2012).
17. S. Ramirez et al., *Science* **341**, 387–391 (2013).
18. R. L. Redondo et al., *Nature* **513**, 426–430 (2014).
19. C. A. Denny et al., *Neuron* **83**, 189–201 (2014).
20. K. Z. Tanaka et al., *Neuron* **84**, 347–354 (2014).
21. K. K. Cowansage et al., *Neuron* **84**, 432–441 (2014).
22. L. G. Reijmers, B. L. Perkins, N. Matsuo, M. Mayford, *Science* **317**, 1230–1233 (2007).
23. R. L. Clem, R. L. Huganir, *Science* **330**, 1108–1112 (2010).
24. A. Suzuki et al., *J. Neurosci.* **24**, 4787–4795 (2004).
25. B. N. Armbruster, X. Li, M. H. Pausch, S. Herlitze, B. L. Roth, *Proc. Natl. Acad. Sci. U.S.A.* **104**, 5163–5168 (2007).
26. J. H. Han et al., *Science* **323**, 1492–1496 (2009).
27. J. R. Misanin, R. R. Miller, D. J. Lewis, *Science* **160**, 554–555 (1968).
28. K. Nader, G. E. Schafe, J. E. Le Doux, *Nature* **406**, 722–726 (2000).
29. X. Liu, S. Ramirez, S. Tonegawa, *Philos. Trans. R. Soc. Lond. B Biol. Sci.* **369**, 20130142 (2014).
30. A. Besnard, S. Laroche, J. Caboche, *Brain Struct. Funct.* **219**, 415–430 (2014).
31. J. Hall, K. L. Thomas, B. J. Everitt, *Eur. J. Neurosci.* **13**, 1453–1458 (2001).
32. J. L. McGaugh, *Science* **153**, 1351–1358 (1966).
33. Y. Dudai, *Annu. Rev. Psychol.* **55**, 51–86 (2004).
34. J. P. Johansen, C. K. Cain, L. E. Ostroff, J. E. LeDoux, *Cell* **147**, 509–524 (2011).
35. R. R. Miller, L. D. Matzel, *Learn. Mem.* **13**, 491–497 (2006).
36. C. A. Miller, J. D. Sweatt, *Learn. Mem.* **13**, 498–505 (2006).
37. S. Chen et al., *eLife* **3**, e02844 (2014).
38. S. Nabavi et al., *Nature* **511**, 348–352 (2014).
39. D. O. Hebb, *The Organization of Behavior; A Neuropsychological Theory* (Wiley, New York, 1949).
40. S. Daumas et al., *Learn. Mem.* **15**, 625–632 (2008).

COGNITIVE NEUROSCIENCE

Unlearning implicit social biases during sleep

Xiaoqing Hu,[1,2] James W. Antony,[1,3] Jessica D. Creery,[1] Iliana M. Vargas,[1] Galen V. Bodenhausen,[1] Ken A. Paller[1]*

Although people may endorse egalitarianism and tolerance, social biases can remain operative and drive harmful actions in an unconscious manner. Here, we investigated training to reduce implicit racial and gender bias. Forty participants processed counterstereotype information paired with one sound for each type of bias. Biases were reduced immediately after training. During subsequent slow-wave sleep, one sound was unobtrusively presented to each participant, repeatedly, to reactivate one type of training. Corresponding bias reductions were fortified in comparison with the social bias not externally reactivated during sleep. This advantage remained 1 week later, the magnitude of which was associated with time in slow-wave and rapid-eye-movement sleep after training. We conclude that memory reactivation during sleep enhances counterstereotype training and that maintaining a bias reduction is sleep-dependent.

Social interactions are often fraught with bias. Our preconceptions about other people can influence many types of behavior. For example, documented policing errors have repeatedly shown the potential harm of racial profiling (1). In experiments that used a first-person-shooter videogame, both White and Black participants were more likely to shoot Black than White individuals, even when they held a harmless object rather than a gun (2). When hiring potential research assistants, both male and female faculty members were more likely to hire male than equally qualified female candidates (3).

Although the tendency for people to endorse racist or sexist attitudes explicitly has decreased in recent years (4), social biases may nevertheless influence people's behavior in an implicit or unconscious manner, regardless of their intentions or efforts to avoid bias (5). Ample evidence indicates that implicit biases can drive discriminatory behaviors and exacerbate intergroup conflict (5–8). For instance, implicit racial biases decrease investments given to racial out-group members

[1]Department of Psychology, Northwestern University, Evanston, IL 60208, USA. [2]Department of Psychology, University of Texas at Austin, Austin, TX 78712, USA. [3]Princeton Neuroscience Institute, Princeton University, Princeton, NJ 08544, USA.
*Corresponding author. E-mail: kap@northwestern.edu